Journal of the Korean Society
for Marine Environmental Engineering
Vol.1, No.2, pp.82~95, Aug. 1998

A Study on Rescue Technique and Safe Tow of Damaged Ship (2)

- Failure Mechanisms of Collision and Grounding of Double Hull Tanker -

by

Sang-Gab Lee[1], Kyung-Sik Choi[2] and Kyoung-Ho Shon[2]

손상된 선박의 구난 기술 및 안전 예항에 관한 연구 (2)

- 이중선체 유조선의 충돌 및 좌초에 의한 손상역학거동 -

이 상갑[1], 최 경식[2], 손 경호[2]

Abstract

In this paper, two series of numerical simulations are performed using LS/DYNA3D: The first series of numerical simulations are collision events between a 310,000 DWT double hull VLCC (struck ship) and two 35,000 and 105,000 DWT tankers (striking ships). Collisions are assumed to occur at the middle of the VLCC with the striking ships moving at right angle to the VLCC centerline. The second ones, grounding accidents of two 40,000 DWT Conventional and Advanced Double Hull tanker bottom structures, CONV/PD328 and ADH/PD328 models. The overall objective of this study is to understand the structural failure and energy absorbing mechanisms during collision and grounding events for double hull tanker side and bottom structures, which lead to the initiation of inner shell rupture and cause the kinetic energy dissipation to bring the ship to a stop. These numerical simulations will contribute to the estimation of damage extents of collision and grounding accidents and the future improvements in tanker safety at the design stage.

요 약

이 논문에서는 LS/DYNA3D를 이용하여 다음과 같은 2가지 수치 시뮬레이션을 수행한다: 첫 번째 시뮬레이션은 310,000 DWT 이중선체 VLCC (피충돌선)과 35,000 및 105,000 DWT의 2척의 유조선(충돌선)들과의 충돌에 관한 경우로서, 충돌선들은 VLCC의 중심선에 직각으로 중앙부에 충돌하는 것으로 가정한다. 두 번째는 40,000 DWT급의

(1) 정회원, 한국해양대학교 조선해양공학부
(2) 한국해양대학교 조선해양공학부

재래식과 개량식 이중선체 유조선의 선저구조의 2가지 모델, CONV/PD328과 ADH/PD328에 대한 좌초에 관한 시뮬레이션이다. 이 연구의 전체적인 목적은 이중선체 유조선의 선측 및 선저구조에 충돌 및 좌초가 각각 발생하는 동안에 이중선체의 내판이 찢어지기 시작하고 운동에너지가 소산되면서 선체가 정지되는 등의 구조적인 파손 및 흡수에너지의 역학적인 거동을 이해하는 것이다. 이러한 수치 시뮬레이션을 통하여 충돌 및 좌초시의 손상 정도를 쉽게 추정할 수 있을 것이고 유조선의 설계 시 안전도의 개선에 이바지할 수 있게 할 것이다.

Keywords: collision and grounding, numerical simulation, LS/DYNA3D, srtuctural failure mechanism, energy absorbing mechanism.

1. Introduction

Since the Exxon Valdez grounding in 1989 focused international attention on oil spills, the United States of America required a double hull for future tankers in 1990 and IMO adopted similar, though a little bit relaxed regulations in 1992. Exxon Valdez was ordered to pay $5 billion in punitive damages in 1996, in addition to the already spent $2.5 billion for cleanup. This kind of large oil spill accidents can be shown to drive shipping company into bankruptcy. The effort to prevent oil outflow with an improved structural design is quite important, as well as structural analyses during and after collision and grounding accidents, including consideration of residual strength to permit salvage and rescue operation.

In the analysis of accident behavior, a global approach, such as Minorsky's formula[1], has usually been used. However, recent researches show that good prediction and design optimization require the considerations of the behavior and failure mode of structural components, which indicates their importances of resistance against collision and grounding, and also shows their design modification for better performance in collision and grounding. Since the ruptures of inner side shell and inner bottom shell due to collision and grounding are critical failure modes, the informations on the energy absorption capacity up to the above failures might be used as a basis to design and to optimize the structure of double hull tankers.

Hydrocodes, such as MSC/DYTRAN and LS/DYNA3D, were applied to simulate full scale collision experiments using a coupled fluid-structure simulation[2], and full scale numerical simulations of collision[3,4] and grounding[5] for double hull VLCCs to clarify the behavior of different structural members and to suggest a new design of VLCC side structures during failure as well as energy absorption mechanism. Such a full scale numerical simulation may provide an accurate predictions on energy absorption capacity and failure modes of real-sized ship structures. Several large scale oil tanker grounding experiments performed by the Carderock Division of Naval Surface Warfare Center (CDNSWC) as part of the Advanced Double Hull Technology Project[6~8]. Several design models were evaluated for the 30,000~40,000 ton tanker range at approximately one-fifth scale.

It is desirable to estimate the crashworthiness of ship structures against collision comparing their energy absorption capacities with each other. For this study, several sizes of striking ships with different collision speed are used to collide against each struck VLCC up to failure of inner side shell. There are generally two parameters of concerns for a systematic comparison of the grounding resistance of various double hull bottom designs : The first one is the amount of vertical intrusion(the height of rock tip above the keel) without inner shell rupture, and the second, the amount of energy dissipation which is characteristic of a given structure with inner shell rupture[7]. It is desirable to estimate the crashworthiness of double hull bottom structures against grounding comparing their occurrence times, distances from front bulkhead, heights of rock tip and energy absorption capacities at the initial inner ruptures with each other.

In this paper, two series of numerical simulations are performed using LS/DYNA3D : The first series of numerical simulations are collision events between a 310,000 DWT double hull VLCC (struck ship) and two 35,000 and 105,000 DWT tankers (striking ships). Collisions are assumed to occur at the middle of the VLCC with the striking ships moving at right angle to the VLCC centerline. Collision speeds of each striking ships are varied to find a critical failure modes. The second ones, grounding accidents of two 40,000 DWT Conventional and Advanced Double Hull tanker bottom structures, CONV/PD328 and ADH/PD328 models with the same arrangements, which are scaled the experimental models conducted by CDNSWC by the scale factor 5.33 for the full scale structure.

The overall objective of this study is to understand the structural failure and energy absorbing mechanisms during collision and grounding events for double hull tanker side and bottom structures, which lead to the initiation of inner shell rupture and cause the kinetic energy dissipation to bring the ship to a stop. These numerical simulations will contribute to the estimation of damage extents of collision and grounding accidents and the future improvements in tanker safety at the design stage.

2. Validation of LS/DYNA3D

To validate LS/DYNA3D to use in this study, it is desirable to compare the result of numerical simulation of LS/DYNA3D with that of the first experiment[6] preformed by CDNSWC, a conventional T-5 Paul Buck double hull tanker bottom with transverse and longitudinal framing. Figure 1 shows geometry and construction details for the conventional double hull structure in the 30,000~40,000 ton range at approximately one fifth scale, which

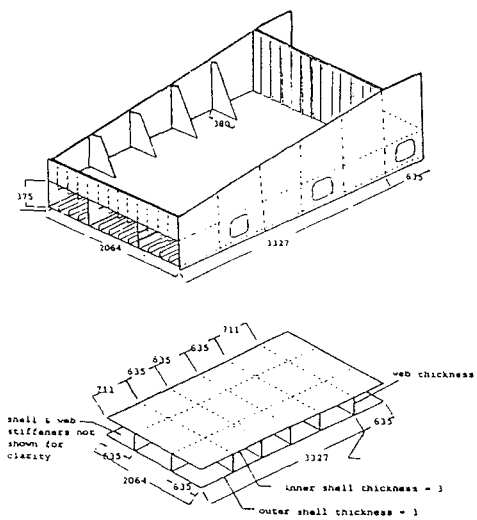

Fig. 1 Dimension of grounding model[6]

consists of the double bottom structure beneath one oil tank, the forward and aft transverse bulkheads, and heavy sideplates. The material used for the grounding model was ASTM A569 with the measured yield and ultimate stresses of 282 MPa and 344 MPa, respectively.

A series of large scale oil tanker grounding experiments have been conducted by CDNSWC using the Grounding Test Machine, which consisted of a 227 tonne test vehicle (or sled) and impact area. Test vehicle built on twin railcars carried the grounding model down an inclined set of railroad tracks to an impact area at a sled velocity of 6.1 m/sec (12 knots). A steel grounding rock included in the impact area was a 914 mm high, 90 degree cone with a 178 mm radius spherical tip. The installation and orientation of the inclined grounding model is shown in Fig. 2 with 7.4 degrees of attack angle and the entry/exit height of the rock tip.

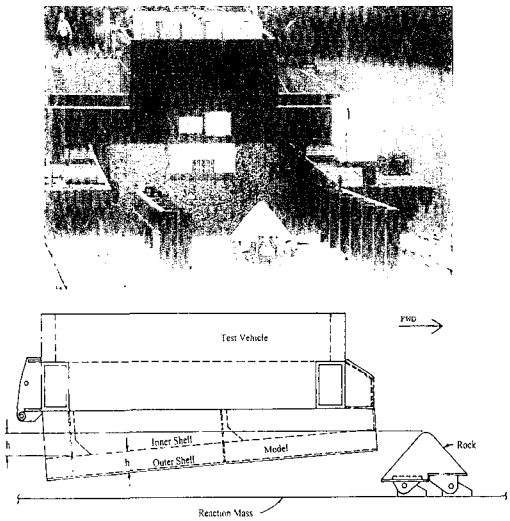

Fig. 2 Installation of grounding model[7]

Figure 3(a) shows the plots of the finite element mesh of grounding double hull structure and grounding rock. All members of inner and outer shells, transverse and longitudinal webs, forward/aft bulkheads, small stiffeners, and grounding rock are modeled using around 18,000 shell elements. The mass of the sled is controlled by rigid plate on the top of the double hull model, which is invisible in Fig. 3. The grounding rock is modeled to be rigid and the double hull model is restrained to move straightly forward, and not upward/ downward.

Material type of strain rate dependent isotropic plasticity is employed for the grounding double hull model, which is suitable for consideration of material dynamic effect.

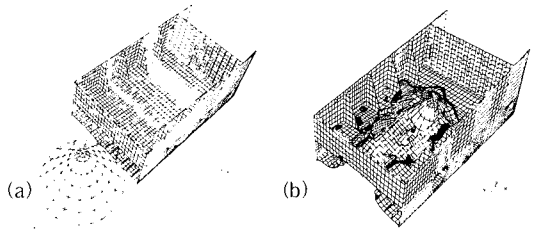

Fig. 3 Finite element mesh and rupture configuration of grounding model

Dynamic yield stress, $\sigma_Y = \sigma_o\{1+(\dot{e}/D)^{1/p}\}$, is used[9], where σ_o is static yield stress, $\dot{e}$ is stain rate, and $D(=40.4\,s^{-1})$ and $p(=5)$ are constants. The density and Poisson's ratio to use here are 7850 kg/m^3 and 0.3, respectively. Every finite element is due to be eliminated when plastic strain reaches to the failure value, 0.25, in this study.

Figure 3(b) shows the configuration of rupture process of the grounding model by the grounding rock. Figure 4 shows the comparison of numerical simulation result with CDNSWC experimental one about the horizontal impact force (plate resisting force) vs. the sled position. Compared to the experimental result, it can be said that the numerical simulation

result is satisfactory and that the already acknowledged tool LS/DYNA3D is sufficient to perform the following collision problems.

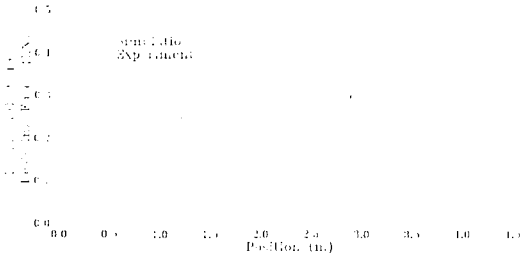

Fig. 4 Comparison of numerical simulation and CDNSWC experimental results

3. Collision Simulations

3.1 Collision scenarios and models

In the considered struck ship, 310,000 DWT D/H VLCC, three tanks are installed across its breadth inside the double hull, cross ties (struts) are fitted in the side tanks and three side stringers are also fitted in the double side,

Table 1 Collision scenarios

Struck Ship 310,000 DWT	Striking Ships			
	35,000 DWT		105,000 DWT	
	5.5 knots	I	4.00 knots	III
	6.0 knots	II	4.25 knots	IV

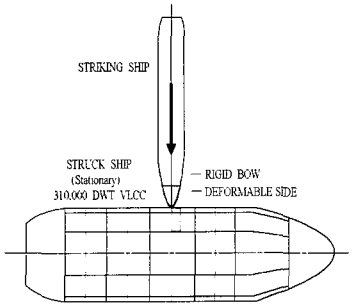

Fig. 5 Numerical model outline

as shown in Fig. 5. When the side of struck ship is hit by the striking ship, cross ties transfer the impact force to the side longitudinal bulkhead. It was reported that the side longitudinal bulkhead showed elastic deformation behavior even while cross ties failed[9]. Collision scenarios considered in this study are shown in Table 1, where striking ships collides against a stationary struck ship in each collision scenario as shown in Fig. 5.

In a high energy collision, large plastic deformations take place in the location of collision on the struck and/or the striking ships, while the rest of both ships show different levels of elastic deformations. Compared to the plastic deformations in the location of collision, the elastic deformations are very small and may be neglected. Therefore, only the regions in both ships containing members expected to show the plastic deformations are modeled as deformable structures, and the rest of both ships, as rigid bodies.

In full scale simulations during collision using MSC/DYTRAN [3], the side of the struck VLCC in the location of collision as well as the bows of the striking ships were modeled as deformable structures, and the rest of the ships, as rigid bodies. The water around the VLCC was modeled with an Eulerian finite volume mesh, and ALE(Arbitrary Lagrangian Euler) coupling was used to couple the water effect to the VLCC. Their results showed that the motions of both striking ship and struck ship were very small with heavy struck ship, and that the effect of the fluid around the struck ship was also small. Damage of the bow of the striking ship was also reported to be relatively smaller than that of the VLCC side[3].

By these results of full scale simulations, in this paper, the effect of the fluid around the struck ship is neglected. Only the deformable structure of the struck ship is employed and the rest of struck ship is neglected. On the assumption that the position of collision is the middle of cargo hold at the center of struck ship, in the longitudinal direction the deformable structure is modeled from the center of struck ship to the two web frames and a symmetric condition is established at the center of cargo hold, as shown in Fig. 5. In the transverse direction, the side longitudinal bulkhead is not modeled due to the level of elastic deformations until the failure of cross ties. Web frame and the shells of deck, bottom and inner bottom connected to the side longitudinal bulkhead are constrained to the transverse direction. Since damage of the bow of the striking ship was reported to be relatively smaller than that of the VLCC side, the bow of the striking ship is modeled as rigid body in this study.

Figure 6 shows the structural members of struck ship VLCC, such as outer side shell, inner side shell, longitudinal stiffener of outer side shell, longitudinal stiffener of inner side shell, No. 1, No. 2, No. 3 webs, No. 1, No. 2, No. 3 stringers, No. 1, No 2, No. 3 cross ties, deck, etc..

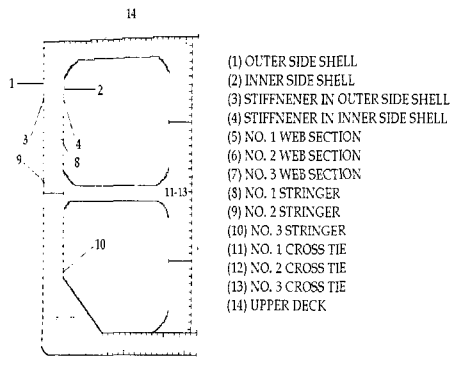

Fig. 6 Structural members of struck VLCC

Figure 7(a) shows the plots of the finite element mesh of the side of struck ship and the bow of 35,000 DWT striking ship, where breadth of side double hull is 3.38 m and space of web section is 5.08 m. The bow of 35,000 DWT striking ship collides against the center of cross tie and its upper deck is located below that of the struck VLCC (scenarios Ⅰ, Ⅱ). In the case of 105,000 DWT striking ship strikes much below the center of cross tie and its upper deck is also located above that of the struck VLCC(scenarios Ⅲ, Ⅳ), as shown in Fig. 7(b). All members of shells, web frames, longitudinal stiffeners, and stringers are modeled using shell element. Around 12,000 shell elements are used in this study.

In collision, tearing of weld lines is usually observed in areas where large damage occurs.

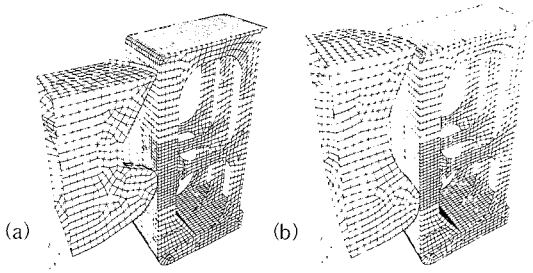

Fig. 7 Finite element mesh of deformable side of struck VLCC and 2 striking ships

Modeling of weld lines and their failure may be necessary in order to accurately predict collision damage. When stresses acting on the weld satisfy a predefined failure condition, the joint breaks up and internal forces are unloaded to the surrounding structure. Since every shell element is complied with failure plastic strain, weld lines are to be neglected in this study.

Strain rate dependent isotropic plasticity material type is also used for the double hull side structures and the material properties used in this study are shown in Table 2.

Table 2 Material properties of models

Density	7850 Kg/m^3
Modulus of elasticity	210 GPa
Poisson's ratio	0.28
Yield stress (mild steel)	250 MPa
Ultimate stress (mild steel)	400 MPa
Dynamic yield stress constants [9]	40.4, 5.0
Failure plastic strain	0.25

In the plane of symmetry, grid points on continuous longitudinal members of the struck ship and the center plane of the striking ship are given symmetric boundary conditions ($U_x = \theta_y = \theta_z = 0.0$). The web frame in the symmetric plane of the struck ship model must contribute only half of its strength to the model. Instead of installation of the side longitudinal bulkhead of the struck ship as the boundary condition, all nodal points at that plane are constrained to the transverse direction. Because of symmetry, only one half of rigid body of bow is explicitly modeled, and the total mass of the striking ship together with 10% added mass is distributed. Simulations of the four scenarios have been carried out, and their results are summarized in the following sections.

3.2 Collision scenarios I & II

Figure 8 shows the deformation and rupture plots of VLCC side with collision speed 6 knots (scenario II) (a) before the failure in the inner side shell(t=1.5sec), (b) after the failure in the inner side shell(t=3.0sec). The bulbous bow penetrates the outer side shell, then the inner side shells at the cross tie of center web frame. It is interesting that the buckling mode of No. 1 cross tie in the tank changes during collision. At the initial stage No. 1 cross ties buckle mainly in bending mode as shown in Fig. 8(a), and at the last stages in Fig. 8(b) the torsional mode of No. 1 cross tie near the collision position can be observed. Since the deck of striking ship collides against the top outer side shell of struck VLCC, its deck penetrates the outer side and inner side shells without rupture of the upper deck of the struck VLCC during collision. The bulbous bow of striking ship with collision speed 5.5 knots(scenario I) pierces the outer side shell and rebounds after the bow arrives at maximum 0.215 m ahead of the inner side shell without rupture of inner side shell. Scenario I shows almost the same trend in the deformation and rupture configuration, as that of Fig. 8(a).

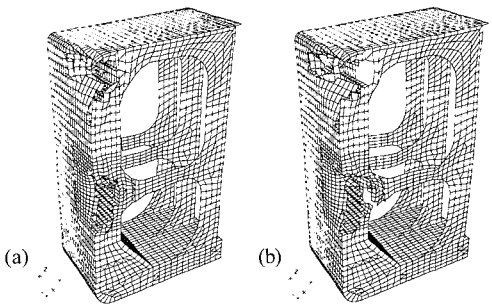

Fig. 8 Deformed side structure in scenario II

Figure 9 shows the variation of collision force with time and penetration in scenario II. It can be seen that failure of the outer side shell starts at time 0.15 sec and the inner side shell initiates to be torn away at time 1.79 sec with maximum deformation, 0.85 m, of the inner side shell.

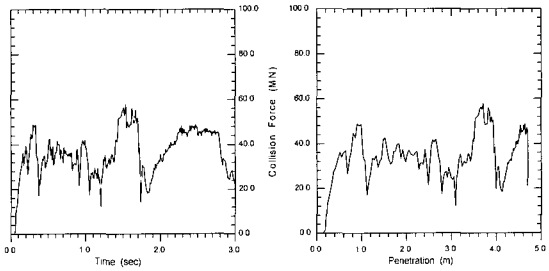

Fig. 9 Collision force variation in scenario II

Figure 10 shows the variation of the total absorbed energy with time and with penetration in scenarios Ⅰ and Ⅱ. It can be seen that the absorbed energy arrives at 159.6 MN-m when the inner side shell begins to be torn away in scenario Ⅱ. It might be thought, therefore, that the critical absorbed energy has to be larger than at least 159.6 MN-m to rupture the inner side shell with 35,000 DWT striking ship at the same position of collision to the struck VLCC as the scenarios Ⅰ and Ⅱ.

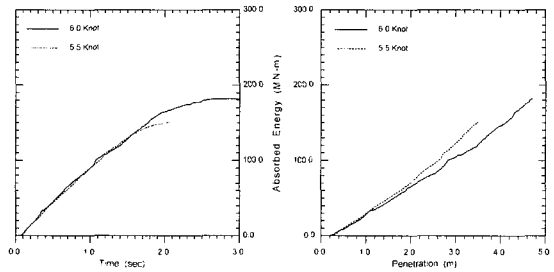

Fig. 10 Total absorbed energy in scenarios Ⅰ & Ⅱ

Figure 11 shows the absorbed energy distribution of each member with time in scenario Ⅱ. Most of absorbed energy are carried by outer side shell, No. 1 web, inner side shell, longitudinal stiffeners of outer and inner side shells, No. 2 web, and No. 2 stringer in capacity sequently during collision, while deck does not contribute to collision in this scenario. This might be due that the deck of the striking ship collides against below the deck of the struck VLCC.

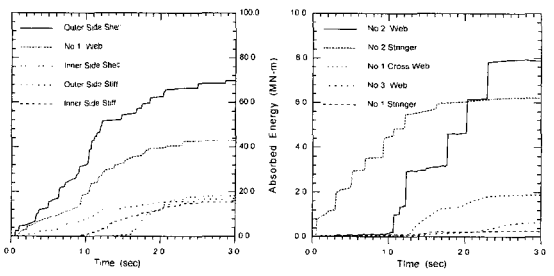

Fig. 11 Energy distribution in scenario Ⅱ

3.3 Collision scenarios Ⅲ & Ⅳ

Figure 12 shows the deformation and rupture plots of VLCC side with collision speed 4.25 knots (scenario Ⅳ) (a) before the failure in the inner side shell (t=2.0sec), (b) right after the failure in the inner side shell (t=2.3sec). The bulbous bow of striking ship crashes the outer side shell between cross tie and hopper tanker, and the upper deck of striking ship collides upward against the deck of struck VLCC. The scope of rupture at the corner between upper deck and top outer side shell of the struck VLCC is much smaller than that of scenario Ⅱ.

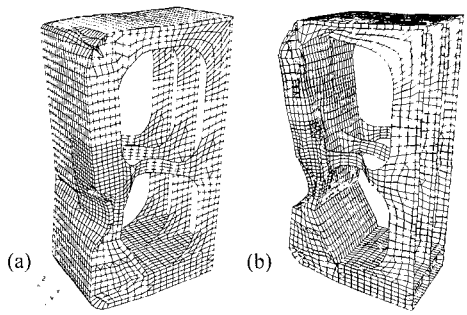

Fig. 12 Deformed side structure (scenario Ⅳ)

While the local rupture in the struck VLCC occurs in scenario Ⅱ, the global damage and rupture occur in scenario Ⅳ. Besides the failure in the inner side shell around the cross tie in scenario Ⅳ, the rupture can be found in the conjunction with hopper tank and inner bottom shell. All cross ties of the struck VLCC buckles more seriously than that of scenario Ⅱ, as shown in Fig. 12. Compared to the case of scenario Ⅱ, the buckling modes of all cross ties occur during rupture of the outer side shell, as shown in Fig. 12(b), which is due to the larger contact area of bulbous bow of 105,000 DWT striking ship than that of 35,000 DWT one. Extreme bending and torsional buckling modes in all cross ties can be found

during the rupture of inner side shell, as shown in Fig. 12(b).

Figure 13 shows the variation of collision force with time and penetration in scenario Ⅳ. It can be seen that the failure of the outer side shell starts at time 0.55 sec and that of the inner side shell, at time 2.28 sec with maximum deformation, 2.4 m, of the inner side shell. The maximum collision force in this case is almost the same as that of scenario Ⅳ, and is much larger (almost 2 times) than that of scenario Ⅱ. It is known that mass of the striking more dominates the collision force than its collision speed does, even though scenario Ⅳ has about 1.5 times as large as scenario Ⅱ in intial kinetic energy. This might be due to the flexibility of impact position of struck VLCC, such as the location between hopper tanker and cross tie of the struck VLCC.

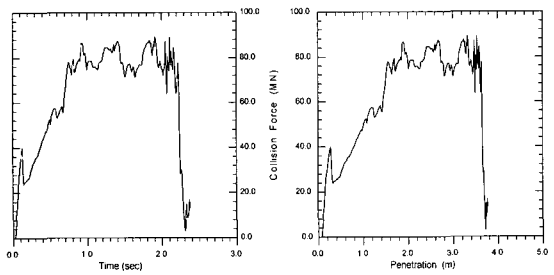

Fig. 13 Collision force variation in scenario Ⅳ

The variation of the total absorbed energy with time and penetration in scenarios Ⅲ and Ⅳ can be found in Fig. 14. In this case the bulbous bow of striking ship reaches the inner side shell with rupture beyond 230.0 MN-m. Figure 15 shows the absorbed energy distribution of each members with time in scenario Ⅳ. Most of absorbed energy are carried by outer side shell, No. 1 web, No. 2 web, No. 3 web, longitudinal stiffeners of outer side shell, deck, No. 3 stringer, No. 2 stringer, and longitudinal stiffeners of inner side shell in capacity sequentially. The contribution of outer side shell in scenario Ⅳ is less than that of scenario Ⅲ, and the others are almost the same level as those of scenario Ⅲ.

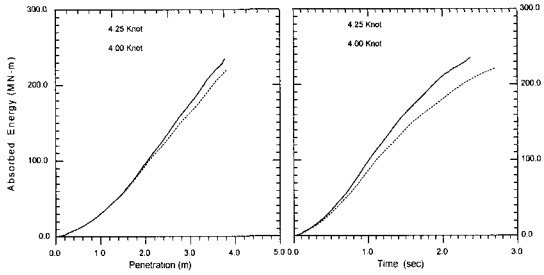

Fig. 14 Total absorbed energy in scenarios Ⅲ & Ⅳ

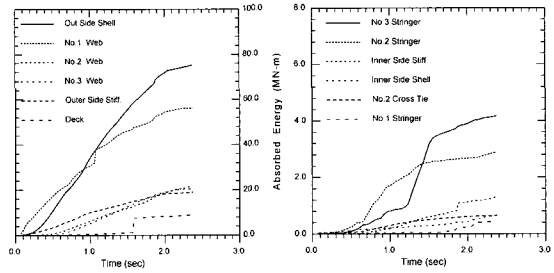

Fig. 15 Energy distribution in scenario Ⅳ

4. Grounding Simulations

4.1 Grounding scenarios and models

Figure 16 shows plots of finite element meshes of two numerical simulation models and grounding rock, which consist of the double bottom structure beneath one and half oil tanks, the forward and aft transverse bulkheads, and heavy sideplates: Conventional double hull tanker bottom design and Advanced (unidirectional) Double Hull(ADH) tanker bottom system. The first CONV/PD328 model, as illustrated in Fig. 16(a), represented the Conventional Double Hull design, whose bottom structure is identical to the MARAD PD328[7,8]. The second Advanced Double Hull model ADH/PD328 model was a rigorously designed alternative to the conventional

MARAD PD328, which is characterized by a tighter spacing of longitudinal webs, double plate transverse bulkheads with haunted stools [7,8]. All members of grounding models and grounding rock are meshed using shell elements with 22,000 for CONV/PD328 and 16,000 for ADH/PD328. The mass of the sled is controlled by rigid plate on the top of the double hull model, which is invisible together with left sideplate as shown in Fig. 16.

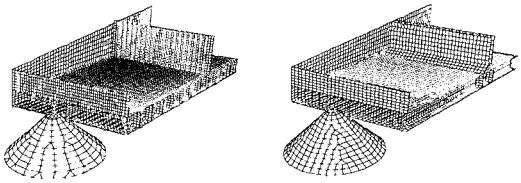

(a) CONV/PD328 (d) ADH/PD328

Fig. 16 Finite element mesh of grounding models

Table 3 Dimensions of grounding models

Item (m)	CONV/PD328	ADH/PD328
Width	13.538	13.538
Length	19.507	19.507
Fwd height	4.642	4.212
Bottom height	1.972	1.972
Shell thickness	0.016	0.016
Stiffener thickness	0.016	0.016
Trans. web thickness	0.016	—
Longi. web thickness	0.0123	0.016
Side plate thickness	1.35	1.35

These simulation models are modified from the experimental ones for the same sizes and impact speed 7.20 m/sec (14.0 knots) for systematic comparisons with each other. Their general dimensions are also illustrated in Table 3, which are scaled by the scale factor 5.33 for the full scale structure. The same material type as that of collision is used.

4.2 Grounding scenarios

Figures 17 and 18 show the rupture configurations of the grounding models by the grounding rock, such as (a) inner shell rupture initiation, (b) bottom structure rupture at the initiation of inner shell rupture, (c) webs and frames rupture at the initiation of inner shell rupture, and (d) inner shell rupture at final simulation time(t=4.5sec).

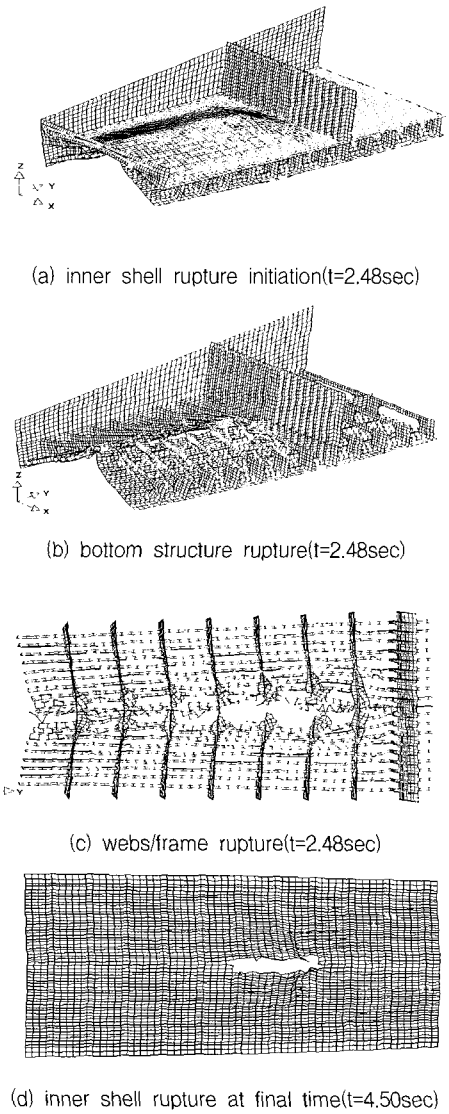

(a) inner shell rupture initiation(t=2.48sec)

(b) bottom structure rupture(t=2.48sec)

(c) webs/frame rupture(t=2.48sec)

(d) inner shell rupture at final time(t=4.50sec)

Fig. 17 Rupture configuration of grounding model, CONV/PD328

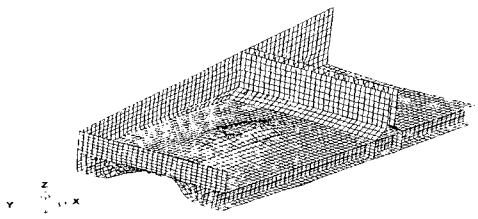

(a) inner shell rupture initiation(t=2.20sec)

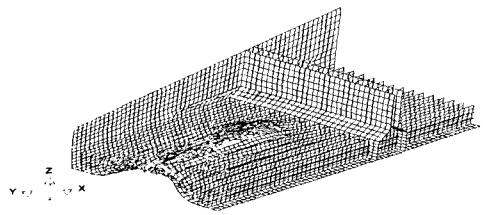

(b) bottom structure rupture(t=2.20sec)

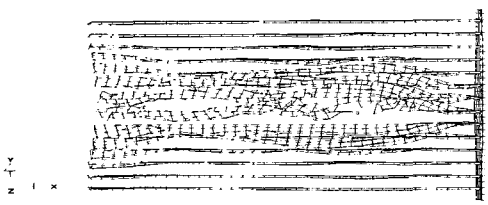

(c) webs/frame rupture(t=2.20(sec)

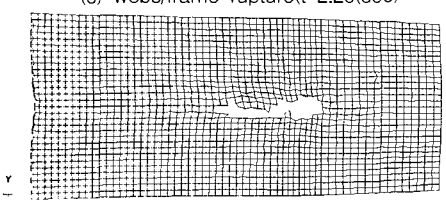

(d) inner shell rupture at final time(t=4.50sec)

Fig. 18 Rupture configuration of grounding model, ADH/PD328

Figures 19 and 20 show the plots of vertical and fore/aft collision forces with respect to the rock tip position for the grounding models until final simulation time t=4.5 sec, respectively. Total absorbed energy and velocity histories with an initial velocity 7.20 m/sec(14 knots) are also plotted with respect to the rock tip position in Fig. 21. Figure 22 shows each member absorbed energy of the grounding models with respect to the rock tip position. Dot point(·) on the graphs through Figs. 19~22 indicates the state of initiation of inner shell rupture. Many informations at the initiation of inner shell rupture of grounding models are summarized in Table 4, such as occurrence time, distances from front bulkhead, height of rock tip, vertical and fore/aft collision forces, absorbed energy, addition to the rock tip position and velocity at final simulation time.

Table 4 Informations at initiation of inner shell rupture of grounding models

Item	CONV/PD328	ADH/PD328
Time(sec)	2.48	2.20
Rock tip position(m)	17.001	14.911
Rock tip height(m)	3.565(1.805)	3.329(1.703)
Vertical Collision Force(MN)	51.4841	47.8089
Fore/Aft Collision Force(MN)	44.008	35.763
Absorbed Energy(MN-m)	249.432	330.987
Rock tip position(m) t=4.5sec	28.051	26.062
Velocity(m/sec) t=4.5sec	4.890	3.950

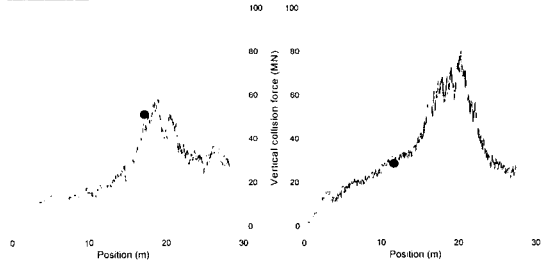

(a) CONV/PD328 (b) ADH/PD328

Fig. 19 Vertical collision forces

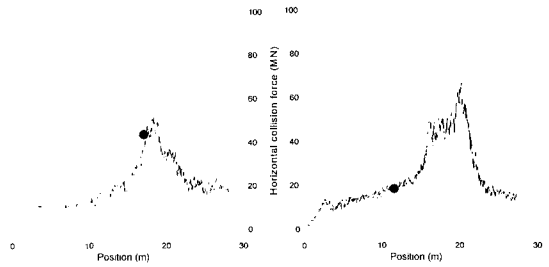

(a) CONV/PD328 (b) ADH/PD328

Fig. 20 Fore/Aft collision forces

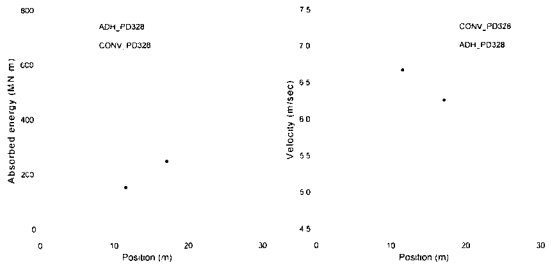

(a) Absorbed energy (d) Velocity

Fig. 21 Absorbed energies and velocities

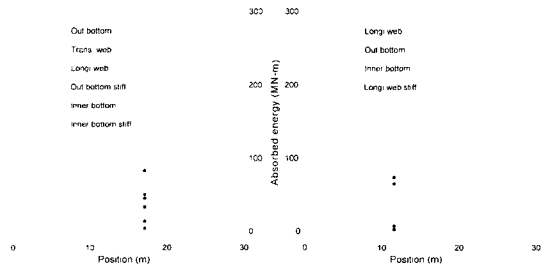

(a) CONV/PD328 (b) ADH/PD328

Fig. 22 Member absorbed energies

The vertical and fore/aft collision forces of CONV/PD328 model in Figs. 19(a) and 20(a) show that distinctive force fluctuations does not clearly mark the locations of 7 transverse webs. Collision forces increase sharply after the 7th transverse web rupture at 16.498m(2.40sec) and then inner shell rupture at 17.001m(2.48sec), as shown in Figs. 17(a)~(c). Figure 21(a) shows the variation of total absorbed energy with respect to the position of rock tip, and Fig. 21(b), the velocity. The vertical and fore/aft collision forces of ADH/PD328 model in Figs. 19(b) and 20(b) are larger than CONV/PD328 model, except partly around at final simulation time. As shown in Figs. 21(a) and (b), their total absorbed energies have the same trends as their collision forces, and rate of velocity decrease of the former is more steeper than the latter. This means ADH/PD328 model is better crashworthy against grounding events than CONV/PD328 one globally.

As shown in Figs. 18(a)~(c), however, the initiation of inner shell rupture of ADH/PD328 model occurs at shorter distance 14.911m (2.20sec) with lower height of rock tip 3.329m than CONV/PD328 one. As shown in Figs. 17(c) and 18(c), the side bottom stiffeners and transverse webs of CONV/PD328 model can be seen to bend largely, which means that this bottom structure is better connected against crash than ADH/PD328 model. This might be guessed that the bottom structure system of the CONV/PD328 model is more flexible and better crashworthy at the initiation of the inner shell rupture, that is, locally. As illustrated in Figs. 17(d) and 18(d), it can be seen that inner shell rupture of CONV/PD328 model continued to the second tanker right after the aft bulkhead, whereas inner shell rupture of ADH/PD328 model stopped at the aft bulkhead, which might be the structural feature of its double plate bulkhead to the bottom shell with haunted stool. This also indicates that the bottom structure system of the CONV/PD328 model is better crashworthy than that of ADH/PD328.

The variations of member absorbed energies are shown in Figs. 22(a) and (b). The following members are contributed to the crashworthiness in CONV/PD328 model, such as outer shell, transverse web, longitudinal web, outer shell stiffeners, inner shell and inner shell stiffener in sequence, whereas in ADH/PD328 model, the members of longitudinal webs and their stiffeners are more contributed to the crashworthiness than outer shell.

5. Summary and Conclusion

Two series of numerical simulations are performed using LS/DYNA3D: Full scale

numerical simulations of collision for the struck 310,000 DWT double hull VLCC with two striking 35,000 and 105,000 DWT tankers, numerical simulations of grounding events of two 40,000 DWT Conventional and Advanced Double Hull tanker bottom structures. It might be thought that it was useful to use full numerical simulation to assess the structural failure mechanisms and the informations about the energy absorption capacity, for which large or full scale experiments are difficult and not practical. The following observations from the numerical simulations can be obtained:

- It has been observed that the structural failure behavior and the absorbed energy greatly depend on the location of collision on the side structure(collision contact direction between striking and struck ships, flexibility of struck ship structure at collision region) and shape of sticking ship(collision contact area), besides the mass and speed of striking ship.
- According to the numerical simulations of this study, the critical collision speeds of 310,000 DWT struck VLCC can be estimated just below 6.0 knots for 35,000 DWT, and about 4.25 knots for 105,000 DWT striking ships. Intial kinetic energy is increased as the mass of striking ship is increased, where the initial kinetic energy of 105,000 DWT of striking ship with speed 4.25 knots is about 1.5 times as large as that of 35,000 DWT one with speed 6.0 knots.
- As expected, the collision force of 35,000 DWT of striking ship is much less than that of 105,000 DWT one, and the absorbed energy of the former for fracture of inner side shell is much less than that of the latter. While the local rupture in struck VLCC occurs at the collision with relative small striking ship (35,000 DWT), the global damage and rupture happen to at the collision with large one (105,000 DWT). From these results, the following comment might be obtained that this type of 310,000 DWT struck VLCC has the failure modes in the inner side shell with lower absorbed energy from local rupture (35,000 DWT) than from global deformation and rupture (105,000 DWT) during collision.
- Structural members, such as outer side shell and No.1 web of 310,000 DWT struck VLCC sustain almost the absorbed energy. As the local rupture occurs rather than the global deformation and rupture, the inner members, such as inner side shell and longitudinal stiffener of inner side shell, support the absorbed energy partly.
- Rupture initiation takes place as soon as the intruding rock creates a high inner shell membrane stresses. Rupture of inner shell can be delayed as long as the connectivity of whole bottom structure is much better to deform globally.
- Over the final simulation time t=4.5sec, ADH/PD328 model dissipated more energy than CONV/PD328 model, and rate of its velocity decrease was also steeper. By the point of energy dissipation, ADH/PD328 model can be considered to be a crashworthy design globally.
- CONV/PD328 model is more crashworthy design locally in that initiation of inner shell rupture occurred at longer distance from fore bulkhead with higher height of rock tip intrusion than ADH/PD328 model. And inner shell rupture stopped at the second tank right after the aft bulkhead compared to the continued rupture of CONV/PD328 model. This model had more energy dissipation and larger grounding resistant force at the initiation of inner shell rupture.

- The members of outer shell and transverse webs are largely contributed to the crashworthiness in Conventional double hull bottom structures, whereas the members of longitudinal webs were more contributed than outer shell member in Advanced Double Hull ones.
- For the future study, realization of optimized double hull side and bottom structures against collision and grounding will be performed, through the simulations using more various side and bottom designs, various arrangements of members, and change of their sizes and thicknesses.

Acknowledgements

The authors wish to acknowledge of the financial support of the Korea Research Foundation made in the Program Year 1997.

References

[1] V. U. Minorsky, "An analysis of ship collision with reference to protection of nuclear power plants", J. of Ship Research, 1959.

[2] H. Lenselink et. al., "A 3-dimensional numerical simulation of the full scale Dutch-Japanese full scale ship collision tests with ALE fluid-structure interaction", FEM WORLD CONFERENCE, Monte Carlo, November 1993.

[3] J.Y. Kim, K.J. Lee, J.M. Kang, D.H. Kim, S. Rashed and D. Xiang, "Behavior of double hull VLCCs in collision", PRADS '95, September 1995.

[4] Ou Kitamura, "Comparative study on collision resistance of side structure", Int. Conference on Designs and Methodologies for Collision and Grounding Protection of Ships, August 1996.

[5] J.S. Che et. al., "Numerical simulations of double hull VLCC in grounding events", Samsung Heavy Industry, December 1994.

[6] James L. Rodd and Jerome P. Sikora, "Double hull grounding experiments", Proc. of the 5th Int. Offshore and Polar Eng. Conference, The Hague, The Netherlands, June 1995.

[7] James L. Rodd, "Large scale tanker grounding experiments", Proc. of the 6th Int. Offshore and Polar Eng. Conference, Los Angeles, USA, May 1996.

[8] James L. Rodd, "Observations on Conventional and Advanced Double Hull grounding experiments", SNAME/SNAJ Conference, August 1996.

[9] G.R. Cowper and P.S. Symonds, "Strain-hardening and strain-rate effects in the impact loading of cantilever beams", Tech. Report No. 28, Brown University, Rhode Island, 1957.